

A nalytical P redictions for Statistics of C osmic Shear: T ests A gainst S imulations

Patrick Valageas¹, Andrew J. Barber², Djipak Munshi^{3,4}

¹ Service de Physique Théorique, CEA Saclay, 91191 Gif-sur-Yvette, France

² A stronom y C entre, University of Sussex, Falmer, Brighton, BN1 9Q J, United Kingdom

³ Institute of A stronom y, M adingley Road, Cambridge, CB3 0HA, United Kingdom

⁴ A strophysics G roup, Cavendish Laboratory, M adingley Road, Cambridge CB3 0HE, United Kingdom

21 February 2019

A B S T R A C T

Weak gravitational lensing surveys are rapidly becoming important tools to probe directly the mass density fluctuations in the universe and its background dynamics. Earlier studies have shown that it is possible to model the statistics of the convergence field on small angular scales by suitably modeling the statistics of the underlying density field in the highly non-linear regime. We extend such methods to model the complete probability distribution function, PDF, of the shear as a function of scattering angle. Our model relies on a simple hierarchical Ansatz for the behaviour of the higher-order correlations in the density field. We compare our predictions with the results of numerical simulations and find excellent agreement for different cosmological scenarios. Our method provides a new way to study the evolution of non-Gaussianity in gravitational clustering and should help to break the degeneracies in parameter estimation based on analysis of the power spectrum alone.

K ey w ords: C osmology: theory { gravitational lensing { large-scale structure of U niverse **M**ethods: analytical { M ethods: statistical {M ethods: numerical

1 IN T R O D U C T I O N

Recent detection of weak lensing (see, e.g., Bartelmann & Schneider, 2001, for a review) due to the large-scale structure in the universe has presented a new opportunity to study cosmology (see, e.g., Bacon, Refregier & Ellis, 2000, Hoekstra et al., 2002, Van Waerbeke et al., 2000, and Van Waerbeke et al., 2002). With a tight control on various systematics these studies were able to relate the weak distortions in the images of high-redshift galaxies with the intervening large-scale mass density inhomogeneities in the universe. Such studies which are statistical in nature (as opposed to strong lensing studies) provide us with a unique way to probe the statistical properties of the underlying density distribution. Traditionally, the study of gravitational clustering in the quasi-linear and non-linear regimes was done by analyzing galaxy catalogues and were plagued by the question of bias associated with the galaxy distribution. Now, therefore, one needs a prescription for galaxy bias to relate the galaxy distribution to the underlying dark matter distribution. Gravitational lensing allows us to bypass this problem as it directly probes the mass distribution. Pioneering works in this direction were done by B landford et

al. (1991), M iralda-Escud e (1991), and Kaiser (1992), based on the earlier work by Gunn (1967).

A key tool for the understanding of cosmological weak lensing has been provided by the development of numerical techniques to follow null geodesics in a perturbed model universe. Such numerical studies typically employ N -body simulations through which ray-tracing experiments are conducted (see, e.g., Schneider & Weiss, 1988, Jaroszyn'ski et al., 1990, Lee & Paczyn'ski, 1990, Jaroszyn'ski, 1991, Babul & Lee, 1991, and B landford et al., 1991). Building on the earlier work of W ambsganns et al. (1995 and 1997), detailed numerical studies were done by W ambsganns, Cen & Ostriker (1998). Other recent studies using ray-tracing have been conducted by P remadi, M artel & M atzner (1998), Van Waerbeke, Bernardeau & M ellier (1999), Bartelmann et al. (1998), and W hite & Hu (2000). Recently, C ouchman, Barber & Thomas (1999) have developed a new technique based on computing the full three-dimensional shear at locations along the lines of sight. Their method combines the computed shear matrices to produce the required lensing statistics for sources at the selected redshift. The method is complementary to ray-tracing and has been fully implemented. Excellent agreement between the results obtained

using Couchman et al.'s (1999) method and analytical predictions have been reported by Barber (2002) and Barber & Taylor (2002).

On the other hand, analytical approaches have also been developed to elucidate the link between the statistical distortion of distant sources by weak lensing and the properties of the large-scale structure of the universe. Most of these analytical works have focussed on large smoothing angles where perturbative calculations are valid (e.g., Vittinen, 1996, Stebbins, 1996, Bernardeau et al., 1997, Jain & Seljak, 1997, Kaiser, 1998, Van Waerbeke, Bernardeau & Mellier, 1999, and Schneider et al., 1998). Small angular scales are more difficult to handle since they probe the non-linear regime where the density field can no longer be described through perturbative expansions which start behaving badly (e.g., Valageas, 2002b). Thus, for ongoing surveys with a small sky coverage perturbative results are unlikely to be sufficient. Therefore, we need theoretical predictions at small angular scales where the signal will dominate the noise.

Unfortunately, we lack a complete understanding of the gravitational clustering in the highly non-linear regime since it has not been possible so far to solve the Vlasov-Poisson system which describes the collisionless gravitational dynamics. Nevertheless, several phenomenological models have been developed to describe the non-linear density field. An interesting family of such models, often called 'hierarchical models', assumes a tree hierarchy for many-body correlation functions. Then, each model is specified by the way it assigns weights to trees of the same order but of different topologies (Fry, 1984, Schaefer, 1984, Bernardeau & Schaefer, 1992, and Szapudi & Szalay, 1993 and 1997). Note that the evolution of the two-point correlation function in all such approximations is left arbitrary. On the other hand, independent studies by various authors (Hamilton et al., 1991, and Peacock & Dodds, 1994 and 1996) suggest an accurate

fitting formula for the evolution of the two-point correlation function based on simple non-local scaling arguments. Combining a hierarchical Ansatz with such a non-local scaling for the two-point correlation one obtains a complete statistical description of gravitational clustering in the highly non-linear regime (e.g., Valageas & Schaefer, 1997, Munshi et al., 1999, Munshi, Coles & Melott, 1999a, b, and Munshi, Melott & Coles 1999).

Such an approach was initiated by Hui (1999) for the study of the three point correlation function for convergence maps and was later extended to compute the full probability distribution function (Valageas, 2000a, b, and Munshi & Jain, 2000 and 2001), the associated bias (Munshi, 2000) and the cumulant correlators associated with such distributions (Munshi & Jain, 2000). See also Munshi & Wang (2003) for the extension of these studies to cosmological scenarios with dark energy. Next, such studies were extended to handle the compensated filter appropriate for the aperture-mass, M_{ap} , which is more useful in weak lensing surveys (Bernardeau & Valageas, 2000). Error estimations were also performed based on such a hierarchical Ansatz to optimize survey strategies (Munshi & Coles, 2003), while implications for Type Ia Supernov studies were carried out by Valageas (2000a) and Wang, Holz & Munshi (2002).

So far most analytical calculations have focussed on convergence maps where analytical results are simplified due to the fact that the convergence is a scalar. Similar progress in

the case of the shear was lacking due to the spinorial nature of shear fields. However from an observational point of view, shear maps are a direct outcome of surveys whereas mapping for the convergence field can be problematic due to the non-trivial topology of the survey area. Therefore, extending previous studies of weak gravitational lensing based on hierarchical models, we introduce in this article a model, which we also call a 'stellar model,' to evaluate the probability distribution function, PDF, of the shear. We test our analytical predictions against numerical simulations and we show that our simple model provides a good description of the shear PDF at small angular scales. Our approach is complementary to studies related to lower order statistics of the shear field (Masahiro & Jain, 2003, Zaldarriaga & Scoccimarro, 2003, Schneider & Lombardi, 2003, and Bernardeau, Van Waerbeke & Mellier, 2002) which also aim to detect non-Gaussianity from ongoing surveys.

This paper is organized as follows. Section 2 briefly describes the weak gravitational lensing effects as measured through the convergence, κ , and the shear, γ . In Section 3, we recall the relationship between PDFs and cumulants (which are the basic tools of our analytical method) and we present our model for the many-body density correlations. This allows us to compute in Section 4 the PDFs for the shear components and for the shear modulus. Section 5 contains a brief explanation of the method used to obtain the lensing statistics from the numerical simulations. In Section 6, we make the comparison between these numerical results and our analytical predictions, and we conclude in Section 7 by discussing our results and future work.

2 DISTORTIONS INDUCED BY WEAK GRAVITATIONAL LENSING

2.1 Shear tensor

The gravitational lensing effects produced by density fluctuations along the trajectory of a photon lead to an apparent displacement of the source and to a distortion of the image. Thus, light coming from a direction $\hat{\gamma}$ is deflected by a small angle γ . However, the observable quantities are not the displacements γ themselves but the distortions induced by these deflections, which are given by the symmetric shear matrix (e.g., Jain, Seljak & White, 2000):

$$\gamma_{ij} = \frac{\partial \hat{\gamma}_i}{\partial \hat{\gamma}_j} = 2 \int_0^s d \frac{D(\hat{\gamma}) D(\hat{\gamma}_s)}{D(\hat{\gamma}_s)} r_i r_j (\hat{\gamma}); \quad (1)$$

Here $\hat{\gamma}$ is the radial comoving coordinate (and s corresponds to the redshift, z_s , of the source):

$$d = \frac{\frac{c}{H_0} dz}{1 + (1 - m)(1 + z)^2 + m(1 + z)^3}; \quad (2)$$

while the angular distance D is defined by:

$$D(\hat{\gamma}) = \frac{\frac{c}{H_0} \sinh \frac{\hat{\gamma}}{m} - \frac{\hat{\gamma}}{m}}{\frac{\hat{\gamma}}{m}} = c; \quad (3)$$

where \sinh means the hyperbolic sine, \sinh , if $(1 - m) > 0$, or sine if $(1 - m) < 0$; if $(1 - m) = 0$, then $D(\hat{\gamma}) = \hat{\gamma}$. The gravitational potential, ϕ , is related to the fluctuations of the density contrast, κ , by Poisson's equation:

$$= \frac{3}{2} m \frac{H_0^2}{c^2} (1+z) \quad \text{with} \quad (x) = \frac{(x)}{s}; \quad (4)$$

where m is the mean density of the universe. In eq.(1) we used the weak lensing approximation; the derivatives $r_{ij}(\cdot)$ of the gravitational potential are computed along the unperturbed trajectory of the photon. This assumes that the components of the shear tensor are small but the density fluctuations can be large (Kaiser, 1992). The shear tensor $_{ij}$ is usually decomposed into its trace, γ , and the shear components γ_1, γ_2 , defined by:

$$= \frac{\gamma_{11} + \gamma_{22}}{2} \quad (5)$$

and

$$\gamma_1 = \frac{\gamma_{11} - \gamma_{22}}{2}; \quad \gamma_2 = \gamma_{12}; \quad \gamma = \gamma_1 + i\gamma_2; \quad (6)$$

Note that since the shear components, γ_1 and γ_2 , and their signs can be exchanged through appropriate rotations of the coordinate axes the joint probability distribution function (PDF) $P(\gamma_1, \gamma_2)$ obeys:

$$P(\gamma_1, \gamma_2) = P(j_1 \bar{j}_1 j_2) = P(j_2 \bar{j}_2 j_1); \quad (7)$$

2.2 Convergence:

Using eq.(1) and eq.(4) one can show (Bernardeau et al., 1997, and Kaiser, 1998) that the convergence along a given line of sight is:

$$\gamma = \frac{3}{2} m \int_0^s d w(\cdot, s) (\cdot); \quad (8)$$

with:

$$w(\cdot, s) = \frac{H_0^2}{c^2} \frac{D(\cdot) D(s)}{D(s)} (1+z); \quad (9)$$

where z corresponds to the radial distance s . Thus the convergence, γ , can be expressed in very simply as a function of the density field; it is merely an average of the local density contrast along the line of sight. Then, we can see from eq.(8), that there is a minimum value, $m_{\text{min}}(z_s)$, for the convergence of a source located at redshift z_s , which corresponds to an "empty" beam between the source and the observer ($\gamma = 1$ everywhere along the line of sight):

$$m_{\text{min}} = \frac{3}{2} m \int_0^s d w(\cdot, s); \quad (10)$$

Following Valageas (2000a, b) it is convenient to define the "normalized" convergence, $\hat{\gamma}$, by:

$$\hat{\gamma} = \frac{\gamma}{m_{\text{min}}} = \frac{1}{m_{\text{min}}} \int_0^s d \hat{w}; \quad \text{with} \quad \hat{w} = \frac{w(\cdot, s)}{m_{\text{min}}}; \quad (11)$$

which obeys $\hat{\gamma} \in [-1, 1]$. Here we introduced the "normalized selection function," $\hat{w}(\cdot, s)$. One interest of working with normalized quantities like $\hat{\gamma}$ is that most of the cosmological dependence (on m , s and z_s) and the projection effects are encapsulated within m_{min} , while the statistics of $\hat{\gamma}$ (e.g., its PDF) mainly probe the deviations from Gaussianity of the density field which arise from the non-linear dynamics of gravitational clustering. If one smoothes the observations with a top-hat window in real space of small angular radius, s , one rather considers the "blurred normalized convergence" $\hat{\gamma}_s$ (where the subscript "s" refers to "smoothed"):

$$\hat{\gamma}_s = \frac{1}{s} \int_0^s d \hat{w}(\cdot, s); \quad ; D \# : \quad (12)$$

Here $\#$ is a vector in the plane perpendicular to the line of sight (we restrict ourselves to small angular windows) over which we integrate within the disk $\# j_s$; we note this by the short notation $\#$. Thus s is the radial coordinate, while $D \#$ is the two-dimensional vector of transverse coordinates. Eq.(12) clearly shows that the convergence $\hat{\gamma}_s$ is actually an average of the density contrast over the cone of angular radius s .

In the following, it will be convenient to work in Fourier space. Thus, we define the Fourier transform of the density contrast by:

$$\hat{w}(k) = \int d k e^{i k \cdot x} w(k); \quad (13)$$

where x and k are comoving coordinates. Then, eq.(12) also reads:

$$\hat{\gamma}_s = \frac{1}{s} \int_0^s d \hat{w}(\cdot, s) \int d k e^{i k \cdot x} W(k, D_s)(k); \quad (14)$$

where k_x is the component of k parallel to the line of sight and k_\perp is the two-dimensional vector formed by the components of k perpendicular to the line of sight. Here we introduced the Fourier form $W(k, D_s)$ of the real-space top-hat filter of angular radius s :

$$W(k, D_s) = \frac{1}{s} \int_0^s d \# e^{i k_\perp \cdot \#} = \frac{2 J_1(k_\perp D_s)}{k_\perp D_s}, \quad (15)$$

where J_1 is the Bessel function of the first kind of order 1. If we choose another filter (e.g., a Gaussian window rather than a top-hat) the expression (14) remains valid and we simply need to use the relevant Fourier window $W(k, D_s)$.

2.3 Shear:

For the shear, γ , defined in eq.(6), we can obtain expressions which are similar to eqs.(12)–(14). Thus, from eq.(1) and eq.(6) we obtain in Fourier space for the normalized shear

$$\hat{\gamma} = \frac{1}{m_{\text{min}}} \int_0^s d \hat{w}(\cdot, s) \int d k e^{i k \cdot x} \frac{k_1^2 - k_2^2 + 2i k_1 k_2}{k_1^2 + k_2^2} (k) \quad (16)$$

where k_1 and k_2 are the components of k along the two orthogonal axes perpendicular to the line of sight which also define the directions (1, 2) used in Subsection 2.1 for the components $_{ij}$ of the shear tensor. In eq.(16) we used again the small-angle approximation. Of course, for the smoothed shear $\hat{\gamma}_s$ we get, in a similar fashion to eq.(14):

$$\hat{\gamma}_s = \frac{1}{s} \int_0^s d \hat{w} \int d k e^{i k \cdot x} \frac{k_1^2 - k_2^2 + 2i k_1 k_2}{k_1^2 + k_2^2} W(k, D_s)(k); \quad (17)$$

Going back to real space, we also obtain from eq.(17) for a top-hat filter the expression:

$$\hat{\gamma}_s = \frac{1}{s} \int_0^s d \hat{w} \frac{1}{\#} \int_0^{\#} d \# e^{i 2 \#} (\cdot, D \#); \quad (18)$$

where $\#$ is a vector in the plane perpendicular to the line of sight of length $\#$ and which makes the polar angle, θ , with

the 1-axis (the 2-axis has $\theta = \pi/2$). Note that we integrate over θ over all space outside of the disk of radius s . Thus, the comparison with eq.(12) shows that while the smoothed convergence only depends on the matter within the cone formed by the angular window, s , the smoothed shear only depends on the matter outside this cone.

3 CUMULANTS, PDFS AND MODELS FOR THE MANY-BODY DENSITY CORRELATIONS

In this paper, we wish to evaluate the probability distribution function, PDF, of the shear, γ . To this order, following the approach developed in Valageas (2000a, b) and Munshi & Jain (2000, 2001), we shall first compute the moments (or more precisely the cumulants) of the shear and then obtain the associated PDF. Therefore, we first recall the standard relationship between the PDF and the moment and cumulant generating functions.

3.1 Generating functions

The statistical properties of a random variable s can be obtained from its moment or cumulant generating functions, which are widely used in statistics (see also Balian & Schaeffer, 1989). Thus, the PDF $P(s)$ can be derived from the generating function, $\psi(y)$, defined from the moments, h_s^p , (provided they are finite) by:

$$\psi(y) = \sum_{p=0}^{\infty} \frac{(-1)^p}{p!} h_s^p y^p \quad (19)$$

since we have the inverse Laplace transform :

$$P(s) = \frac{1}{2\pi i} \int_{-i\infty}^{i\infty} \frac{dy}{y} e^{sy} \psi(y) \quad (20)$$

Indeed, the generating function, $\psi(y)$, is simply the Laplace transform of the PDF $P(s)$:

$$\psi(y) = \int_0^{\infty} ds e^{sy} P(s) \quad (21)$$

One can check that expanding the exponential in eq.(21) reproduces eq.(19). If the moments, h_s^p , diverge one can still define $\psi(y)$ from eq.(21) but the expansion at $y = 0$ of the generating function becomes singular. In practice, one usually introduces the generating function, $\psi(y)$, defined from the cumulants, h_s^p , by:

$$\psi(y) = \sum_{p=1}^{\infty} \frac{(-1)^{p-1}}{p!} h_s^p y^p = \ln [\psi(y)] \quad (22)$$

As is well-known, $\psi(y)$ is simply the logarithm of $\psi(y)$. For our purposes, we shall actually use the normalized generating function, $\psi'(y)$, defined by:

$$\psi'(y) = \sum_{p=1}^{\infty} \frac{(-1)^{p-1}}{p!} \frac{h_s^p}{h_s^1} y^p \quad \text{with} \quad s = h_s^2 \quad (23)$$

The comparison of eq.(23) with eq.(22) yields $\psi'(y) = \exp[\psi'(y_s) - s]$, so that eq.(20) now reads:

$$P(s) = \frac{1}{2\pi i} \int_{-i\infty}^{i\infty} \frac{dy}{y} e^{sy} \psi'(y) = s \quad (24)$$

As seen in Section 2, the convergence, γ , or the shear, γ , are given by a linear integral along the line of sight over the density field. In other words, they can be seen as the superposition of independent layers which each contribute to γ or γ .

Indeed, within the small-angle approximation the correlations of the density field will only appear within the transverse directions. Then, the direct calculation of the PDF of such a sum over the redshift of the lenses would yield an infinite number of convolution products which makes it intractable. By contrast, the cumulant generating functions simply add when different layers are superposed (since Laplace transforms change convolutions into ordinary products). This property makes the generating function $\psi'(y)$ a convenient tool to deal with projection effects along the line of sight. This remark is the basis of the method introduced in Valageas (2000a, b). Moreover, the expansion (23) provides a simple way to compute $\psi'(y)$ from the moments (or cumulants) of the random variable one is interested in. This approach can be used for any quantity which is linear over the density field, like the convergence, γ , studied in Valageas (2000a, b), the aperture-mass, M_{ap} , investigated in details in Bernadeau & Valageas (2000) or the shear, γ , we focus on in this paper.

3.2 PDF for the density field

It is clear that in order to derive the PDF of the shear, γ , we need the properties of the underlying density field. A first measure of the statistical properties of the density field is given by the PDF P_R of the density contrast within spherical cells of radius R and volume V :

$$P_R = \frac{1}{V} \int_{-R}^{R} dx \quad (25)$$

Note that the cumulants, h_R^p , can also be written in terms of the many-body connected correlation functions, $\psi_p(x_1; \dots; x_p)$, as (e.g., Peebles, 1980):

$$h_R^p = \frac{1}{p!} \int_V dx_1 \dots dx_p \psi_p(x_1; \dots; x_p) \quad (26)$$

with:

$$\psi_p(x_1; \dots; x_p) = h(x_1) \dots h(x_p) \quad (27)$$

Next, we define the associated normalized generating function, $\psi'(y)$, introduced in eq.(23) and its coefficients, S_p , by:

$$\psi'(y) = \sum_{p=2}^{\infty} \frac{(-1)^{p-1}}{p!} S_p y^p; \quad S_p = \frac{1}{2^{p-1}}; \quad S_2 = 1; \quad (28)$$

which also yields P_R through eq.(24):

$$P_R = \frac{1}{2\pi i} \int_{-i\infty}^{i\infty} \frac{dy}{y} e^{sy} \psi'(y) = \frac{1}{2} \quad (29)$$

Since the convergence, γ_s , is the average of the density contrast, γ , with a smooth positive weight over the relevant cone, its cumulants can be estimated from those of the density field in a robust and simple way, by neglecting their geometrical dependence. Therefore, one merely uses the properties of the density field, P_R , smoothed over spherical cells

and does not take into account the detailed angular dependence of the many-body correlation functions. As shown in Valageas (2000b), this procedure is indeed sufficient to recover the properties of the convergence. In fact, up to a good accuracy, one may even express the PDF, $P(\hat{y}_s)$, directly in terms of the PDF, $P(\hat{y}_R)$, of the density contrast, by using the approximation ' $\hat{y}_s(y) \approx y$ ' (see Valageas 2000b). Here ' \hat{y} ' (also defined in eq.(28)) is the normalized generating function associated with the density contrast R at the scale and redshift which contribute most to the signal, whereas ' \hat{y}_s ' is the normalized generating function associated with the normalized convergence, \hat{y}_s , as defined by eq.(23). This approximation clearly shows that the 'normalized convergence,' \hat{y}_s , mainly probes the non-Gaussianities of the density field (i.e., its very structure) brought by the non-linear gravitational dynamics, while the overall amplitude of the fluctuations (which gives the dependence on the cosmological parameters and the source redshift) is encoded within \hat{y}_s , as we announced earlier, below eq.(11).

3.3 Models for the many-body density correlations

For more intricate filters, this simple approximation is no longer sufficient. This is clearly the case for the shear, since eq.(18) shows that the relevant volume is now the exterior of the cone of radius s , and has a geometry which is significantly different from spherical cells. More importantly, the factor e^{i2} yields a weight often zero and which is both positive and negative and varies with the direction in the transverse plane. This implies that one cannot evaluate the cumulants of these moments of the density field over spherical cells; the natural estimate would be zero, since the angular mean of the weight, e^{i2} , vanishes. The same problem appears for the study of the aperture mass, M_{ap} , which also involves a compensated filter. Therefore, we need an explicit model for the angular dependence of the many-body correlations.

As shown in Bemarreau & Valageas (2000), in the case of the aperture mass, M_{ap} , good results can be obtained at small angles by using a 'minimal tree-model' for the connected correlations of the density field. Let us first recall that a general 'tree-model' is defined by the property (Schaefer, 1984, and Gott & Peebles, 1977):

$$p(x_1; \dots; x_p) = Q_p^{(t)} \prod_{i=1}^{p-1} \langle x_i; x_{i+1} \rangle \quad (30)$$

where (\cdot) is a particular tree-topology connecting the p points without making any loop, $Q_p^{(t)}$ is a parameter associated with the order of the correlations and the topology involved, t is a particular labeling of the topology, (\cdot) , and the product is made over the $(p-1)$ links between the p points with two-body correlation functions. We show in Fig.1 the three topologies which appear within this framework for the 5-point connected correlation function.

3.3.1 Minimal tree model

A peculiar case of the tree-models described by (30) is the minimal tree-model where the weights $Q_p^{(t)}$ are given by Bemarreau & Schaefer (1992):

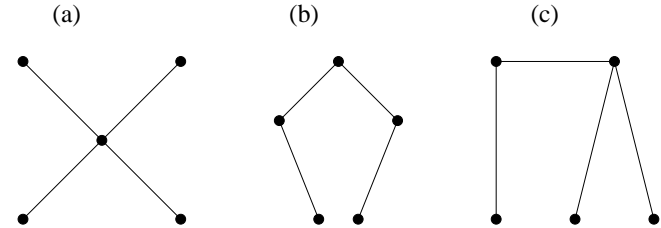


Figure 1. The various topologies one can build for the 5-point connected correlation function within the framework of a tree-model as in (30). Graph (a) is a 'stellar diagram' (i.e., $(p-1)$ points are linked to a central point), while graph (b) is a 'snake diagram' (i.e., one successively visits all points along one curve with only two end-points) and graph (c) is a 'hybrid diagram'.

$$Q_p^{(t)} = \frac{Y}{q} \prod_{q \in \text{vertices of } t} q \quad (31)$$

where q is a constant weight associated to a vertex of the tree topology with q outgoing lines. Then, for an arbitrary real-space filter, $F(x)$, which defines the random variable s as:

$$s = \int dx F(x) \langle x \rangle \quad \text{and} \quad s = hs^2i; \quad (32)$$

it is possible to obtain a simple implicit expression for the normalized generating function, ' $\hat{y}_s(y)$ ' (see Bemarreau & Schaefer, 1992, and Jannink & Des Cloiseaux, 1987):

$$\hat{y}_s(y) = y \int dx F(x) \langle x \rangle \frac{\langle x \rangle^0 \langle x \rangle}{2} \quad (33)$$

$$\langle x \rangle = \frac{Y}{s} \int dx^0 F(x^0) \langle x; x^0 \rangle \langle x^0 \rangle \quad (34)$$

where the function $\langle \cdot \rangle$ is defined as the generating function for the coefficients p :

$$\langle \cdot \rangle = \sum_{p=1}^X \frac{(-1)^p}{p!} p^p \quad \text{with} \quad 1 = 1: \quad (35)$$

Of course, the generating function, ' $\hat{y}_s(y)$ ', depends on the filter, F , which defines the variable, s . For the smoothed density contrast, R , defined in eq.(25), the real-space filter, $F(x)$, is the top-hat of radius R normalized to unity. In this case, a simple 'mean field' approximation which provides very good results (Bemarreau & Schaefer, 1992) is to integrate $\langle x \rangle$ over the volume V in eq.(34) and then to approximate $\langle x \rangle$ by a constant $\langle x \rangle$. This leads to the simple system :

$$\hat{y}_s(y) = y \langle \cdot \rangle \frac{\langle \cdot \rangle}{2} \quad (36)$$

$$= y^0 \langle \cdot \rangle \quad (37)$$

Here and in the following we simply note the generating function associated with the density contrast R as ' $\hat{y}(y)$ ' and we retain suffixes for the generating functions associated with other quantities (e.g., ' \hat{y}_s ' for the shear component, ' \hat{y}_1).

In the case of the aperture mass, M_{ap} , one can still perform the resummation (33)–(34), if the underlying density field is described by such a minimal tree-model, but one can no longer use the 'mean field' approximation (36)–(37)

because the 2-d compensated filter $F(\#)$ now strongly depends on the polar distance $|j|$ (in the 2-d transverse plane). Such a study is described in detail in Bernardeau & Valageas (2000) where it is shown that this minimalist tree-model provides good results when compared with numerical simulations.

Of course, we can apply the same procedure, developed in Bernardeau & Valageas (2000) for M_{ap} , to the shear,

We simply need to use the corresponding real-space filter, F . From eq.(18) we see that this is $F(\#) = H(\# >_s) \cos(2) = \#^2$ for $_1$ and $F(\#) = H(\# >_s) \sin(2) = \#^2$ for $_2$, where H is the Heaviside function with obvious notations. Then, the resummation (33)–(34) yields a two-dimensional non-linear implicit equation which is not very convenient for numerical purposes. Therefore, it is interesting in this case to investigate whether a simpler model for the many-body correlations of the density field could still provide good predictions for the PDF, $P(_1)$, of the shear component, $_{12}$.

3.3.2 Stellar model

Thus, we introduce in this paper a ‘stellar model’, which is a particular case of the tree-models defined in (30), where we only keep the stellar diagrams (e.g., the graph (a) in Fig.1 for the 5-point connected correlation). Thus, the p -point connected correlation $_{p,0}$ of the density field can now be written as:

$$_{p,0}(x_1, \dots, x_p) = \frac{S_p}{p} \sum_{i=1}^p \sum_{j \neq i} \langle x_i^p x_j \rangle: \quad (38)$$

The advantage of the stellar model (38) is that it leads to very simple calculations in Fourier space. Thus, let us define the power-spectrum, $P(k)$, of the density contrast by:

$$h(k_1, k_2) = \delta(k_1 + k_2) P(k_1); \quad (39)$$

where δ is Dirac’s distribution, whence:

$$\langle x \rangle = \int dk e^{ik \cdot x} P(k); \quad (40)$$

Then, eq.(38) reads in Fourier space:

$$h(k_1) \approx \frac{S_p}{p} \sum_{i=1}^p \sum_{j \neq i} \delta(k_1 + k_j) P(k_j); \quad (41)$$

Of course, the Dirac factor, $\delta(k_1 + \dots + k_p)$, simply translates the fact that the many-body correlations are invariant through translations. Therefore, in the following we shall use eq.(41) for the connected correlations of the density field which appear in the calculation of the cumulants of the shear, $_{12}$.

3.4 Amplitude of the density correlations

The stellar model introduced in Section 3.3.2 provides the angular dependence of the many-body correlations of the density field. However, we still need to determine their overall amplitude, that is the non-linear power-spectrum, $P(k)$, and the coefficients, S_p , which enter eqs.(38)–(41). First, we obtain the non-linear evolution of the power-spectrum from the prescription given by Peacock & Dodds (1996), which is

also a good fit to numerical simulations. Second, we determine the coefficients, S_p , as follows. We characterize the amplitude of the density correlations at scale R and redshift z through the parameters S_p defined in eq.(28), which give the amplitude of the many-body correlations over spherical cells of radius R . As seen from eq.(28)–(29) they also define the PDF, $P(R)$. We could obtain these coefficients, S_p , through a parameterization of their generating function, $\langle \dots \rangle$. However, we prefer to specify $\langle \dots \rangle$ through a function (\dots) which is defined by the implicit system (36)–(37). Note that this procedure is merely a convenient parameterization of $\langle \dots \rangle$ and it does not assume by itself a minimalist tree-model. The results recalled in Section 3.3.1 simply mean that in case the actual many-body correlations exactly obey a minimalist tree-model, the function (\dots) defined from eqs.(36)–(37) could also be interpreted as a good approximation to the (slightly different) function (\dots) defined in eq.(35) as the generating function of the vertices $_{p,0}$.

The reason we prefer to parameterize the coefficients, S_p , through (\dots) rather than directly through $\langle \dots \rangle$ is that this procedure was already checked to provide good results in previous works. Thus, it was seen in Bernardeau & Schaeffer (1992) to give good predictions for the galaxy and matter correlations, while in Bernardeau & Valageas (2000) it was shown to yield good predictions for the PDF, $P(M_{ap})$, of the aperture-mass. Since the aperture-mass is closely related to the shear, $_{12}$, we can expect this procedure to give good results for the PDF, $P(_1)$, too. Note however that the calculations developed in Bernardeau & Valageas (2000) used the minimalist tree-model recalled in Section 3.3.1 rather than the stellar model of Section 3.3.2 for the angular dependence of the many-body correlations. Nevertheless, we checked numerically that both models actually give very close results for $P(M_{ap})$. Thus, as in Bernardeau & Valageas (2000) we parameterize (\dots) as:

$$(\dots) = 1 + \dots \quad (42)$$

where we have kept the usual notation, $\langle \dots \rangle$ (not to be confused with the convergence), for the free parameter which enters the definition of (\dots) .

Next, we choose the value of this parameter, $\langle \dots \rangle$, so as to reproduce the skewness, S_3 , in both the highly non-linear and quasi-linear regimes, using the relation:

$$\langle \dots \rangle = \frac{3}{S_3} \quad (43)$$

We take for the skewness in the highly non-linear regime, S_3^{NL} , the prediction of HEPY (Scoccimarro & Frieman, 1999) and for the quasi-linear regime, S_3^{QL} , the exact result obtained from perturbative theory:

$$S_3^{NL} = 3 \frac{4}{1 + 2^{n+1}} \frac{2^2}{7}; \quad S_3^{QL} = \frac{34}{7} (n+3); \quad (44)$$

Here n is the local slope of the linear power-spectrum at the typical scale k and redshift z probed by the measure (defined below eq.(64)). In order to describe intermediate regimes we also introduce the power, $\langle k^2 \rangle$, per logarithmic interval defined as:

$$\langle k^2 \rangle = 4 \int k^3 P(k) dk; \quad (45)$$

Then, for intermediate regimes defined by $1 < \langle k^2 \rangle < \langle k_{vir}^2 \rangle$, we use the simple linear interpolation:

$$S_3 = S_3^{QL} + \frac{\gamma^2(k; z)}{\gamma_{vir}(z)} \frac{1}{1} S_3^{NL} S_3^{QL} : \quad (46)$$

For $\gamma^2(k; z) < 1$ (i.e. the quasi-linear regime), we take $S_3 = S_3^{QL}$, while for $\gamma^2(k; z) > \gamma_{vir}(z)$ (i.e., the highly non-linear regime), we take $S_3 = S_3^{NL}$. Here γ_{vir} is the density contrast at virialization given by the usual spherical collapse (thus $\gamma_{vir} \approx 178$ for a critical-density universe). Indeed, the threshold $\gamma^2 > \gamma_{vir}$ describes the highly non-linear regime where most of the matter at scale $1=k$ has collapsed into non-linear structures.

Finally, as can be seen from eq.(41), the coefficients S_p and S_p' are related by:

$$S_p = S_p' \frac{Z}{dt(3t^2)} \int_0^R \frac{dk}{k} \frac{\gamma^2(k) F(kR) \sin(kRt)}{F^2(kR)} \#_p \quad (47)$$

where we introduced the Fourier transform, $F(kR)$, of a 3-d top-hat of radius R :

$$F(kR) = \frac{dx}{V} e^{ikx} = 3 \frac{\sin(kR)}{(kR)^3} \frac{(kR) \cos(kR)}{(kR)^3} : \quad (48)$$

However, in the following we shall use the simple approximation:

$$S_p' \approx S_p : \quad (49)$$

Alternatively, we may define the function $\gamma'(y)$ obtained from (36)–(37) and our choice of γ as the generating function of the coefficients S_p , rather than S_p , through its Taylor expansion at $y = 0$.

It is interesting to note that the implicit system (36)–(37) appears naturally in the quasi-linear regime. Indeed, as shown in Bemarreau (1994) and Valageas (2002a), in this regime the generating function $\gamma'(y)$ exactly obeys the relation (36)–(37), where γ is closely related to the spherical dynamics for the non-linear density contrast. However, the latter is of the form (42) only in the limit $\gamma \ll 1$ with no smoothing (then, the parameter γ is equal to 3=2). Nevertheless, the form (42) still provides a good approximation for more general cases where γ is adjusted so as to recover the exact skewness. Here we note that the system (36)–(37) usually yields a branch cut along the negative real axis for $y < y_s$ with $y_s \approx 0.1$ for $\gamma'(y)$; see Bemarreau & Schaeffer (1992). For the function γ given in eq.(42) one gets:

$$y_s = \frac{(\gamma + 1)^{+1}}{(\gamma + 2)^{+2}} \quad \text{and} \quad \gamma_s = \frac{1}{\gamma + 2} : \quad (50)$$

Such a singularity leads to an exponential cutoff for the PDF, $P(\gamma_R) \propto e^{-y_s R} \approx e^{-2}$ at large densities. As shown in Valageas (2002a), in the case of the quasi-linear regime this is actually an artefact and one must go through y_s up to a second branch for $\gamma'(y)$, which yields a large density cutoff for $P(\gamma_R)$ which is shallower than a simple exponential. However, it was seen by numerical computations in Valageas (2002a) that this feature does not change the shape of the PDF by much in the range of interest. Moreover, in this paper we are mostly interested in the non-linear regime (which largely dominates for $\gamma < 4^0$ and $z_s = 1$) where the singularity y_s is meaningful and the PDF shows indeed an exponential cutoff (since it is actually defined from the coefficients S_p).

Finally, we must point out that the simple model de-

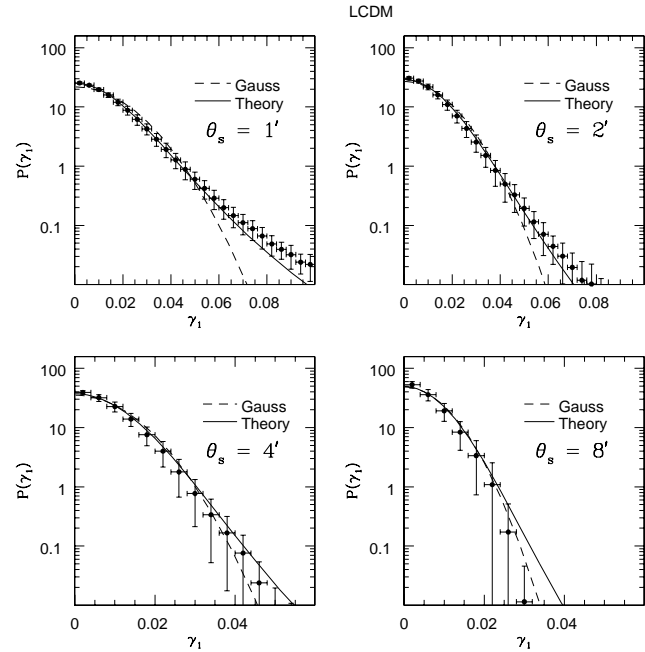


Figure 2. Probability distribution function, $P(\gamma_1)$, for the LCDM cosmology, plotted as a function of γ_1 . The smoothing angle, θ_s , varies from 1^0 (upper left panel) to 8^0 (lower right panel). The data-points are the results from the numerical simulations and the solid lines correspond to the analytical predictions (61) and (63) based on our stellar model. The dashed lines show the Gaussian PDF with the same variance. The source redshift is fixed at unity in each case.

veloped above has no new parameter. Indeed, the power-spectrum evolution is obtained from Peacock & Dodds (1996), while all many-body correlations are defined by the stellar model (38) with their amplitude given by the sole coefficient S_3 (i.e. the skewness of $P(\gamma_R)$) which is exact in the quasi-linear regime and obtained from HEPT (Scoccimarro & Frieman, 1999) in the non-linear regime. In the form given here, our model is obviously consistent with the 'stable-clustering Ansatz' (e.g., Peebles 1980). However, it could incorporate possible deviations from the stable-clustering Ansatz through the non-linear power-spectrum, $P(k)$, or through an additional dependence on redshift and scale for the skewness, S_3 , in the non-linear regime.

4 COMPUTATION OF THE PDFS

4.1 PDF of the shear components, γ_1 and γ_2

We can now use the model developed in Section 3 to describe the density field in order to compute the PDF, $P(\gamma_1)$, of the shear component, γ_1 . First, we obtain from eq.(17):

$$\gamma_{1s} = \frac{Z}{Z_s} \int d\omega dk e^{ik\omega} \cos 2\omega (k, D_s) \gamma(k) : \quad (51)$$

where ω is the polar angle of the transverse vector k . For the component γ_2 we would have $\sin 2\omega$ in place of $\cos 2\omega$.

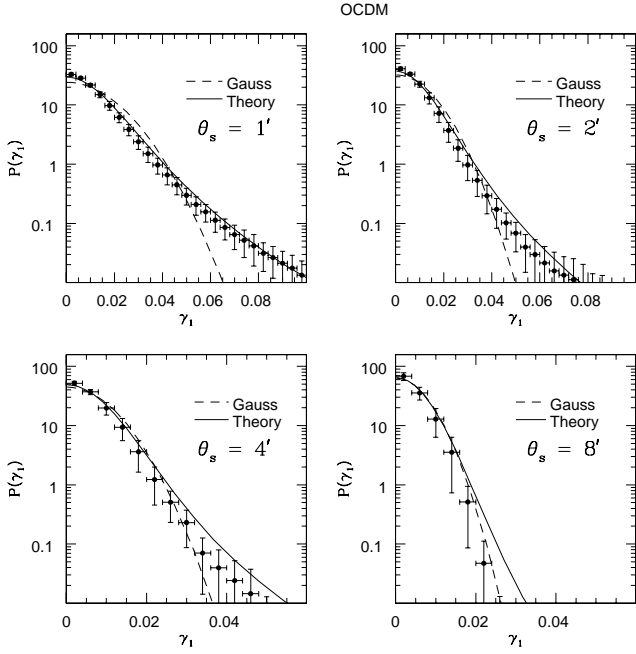


Figure 3. As for the previous Figure, but for the OCDM cosmology.

Then, the cumulant of order p reads:

$$h_{1s}^p i_c = \sum_{i=1}^Z \sum_{j=1}^Z \int d\mathbf{k}_i \hat{w}_i \int d\mathbf{k}_j \cos 2 \int \mathbf{k}_j \mathbf{W}(\mathbf{k}_j D) \int \mathbf{k}_j \mathbf{e}^{i \mathbf{k}_j \mathbf{l}} h(\mathbf{k}_1) \dots h(\mathbf{k}_p) i_c. \quad (52)$$

Since the correlation length (beyond which the density correlations are negligible) is much smaller than the Hubble scale, $c = H(z)$ (where $H(z)$ is the Hubble constant at redshift z), we can simplify eq.(52) as:

$$h_{1s}^p i_c = \sum_{i=1}^Z \sum_{j=1}^Z \int d\mathbf{k}_i \hat{w}_i \int d\mathbf{k}_j \cos 2 \int \mathbf{k}_j \mathbf{W}(\mathbf{k}_j D) \int \mathbf{k}_j \mathbf{e}^{i \mathbf{k}_j \mathbf{l}} S_p D(\mathbf{k}_1 + \dots + \mathbf{k}_p) P(\mathbf{k}_2) \dots P(\mathbf{k}_p); \quad (53)$$

where we used eq.(41). Using the usual small-angle approximation (i.e. $P(\mathbf{k}_j) \approx P(\mathbf{k}_j)$), we can perform the integration over $\mathbf{k}_2, \dots, \mathbf{k}_p$ and $\mathbf{k}_{k1}, \dots, \mathbf{k}_{kp}$, which yields:

$$h_{1s}^p i_c = S_p \frac{d}{2} (2 \hat{w})^p \int d\mathbf{k}_j \cos 2 \int \mathbf{k}_j \mathbf{W}(\mathbf{k}_j D) D(\mathbf{k}_1 + \dots + \mathbf{k}_p) P(\mathbf{k}_2) \dots P(\mathbf{k}_p); \quad (54)$$

Next, we write the Dirac factor as:

$$D(\mathbf{k}_1 + \dots + \mathbf{k}_p) = \frac{dt}{(2\pi)^2} e^{it:(\mathbf{k}_1 + \dots + \mathbf{k}_p)}; \quad (55)$$

so that eq.(54) reads:

$$h_{1s}^p i_c = S_p \frac{d}{2} (2 \hat{w})^p \int \frac{dt}{(2\pi)^2} \int d\mathbf{k}_1 \dots d\mathbf{k}_p$$

$$Y^p \cos 2 \int \mathbf{k}_j \mathbf{W}(\mathbf{k}_j D) e^{it \mathbf{k}_j \cos 2 \int \mathbf{k}_j} P(\mathbf{k}_1) \dots P(\mathbf{k}_p) \quad (56)$$

where we have dropped the subscript $?$, for the 2-d transverse wavenumbers $\mathbf{k}_?$, and we have noted the polar angle of the vector t . The integration over the angles \mathbf{k}_j yields:

$$Z_2 \int d\mathbf{k}_j \cos 2 \int \mathbf{k}_j e^{it \mathbf{k}_j \cos 2 \int \mathbf{k}_j} = 2 \cos 2 \int t \mathbf{k}_j \quad (57)$$

so that eq.(56) becomes:

$$h_{1s}^p i_c = S_p \int_0^Z \int_0^Z \int_0^Z \frac{dt}{t} t^2 \frac{d}{2} (\cos 2 \int \mathbf{k}_1 \mathbf{W}(\mathbf{k}_1 D) \int_0^Z t \mathbf{J}_2(t \mathbf{k}_1 D) I_1(t; \mathbf{k}_1)^{p-1}) \quad (58)$$

where we have made the change of variable $t = tD$ and we have introduced $I_1(t; \mathbf{k}_1)$ defined by:

$$I_1(t; \mathbf{k}_1) = 4 \int_0^Z dk \mathbf{k} \mathbf{W}(\mathbf{k} D) \mathbf{J}_2(t \mathbf{k} D) P(\mathbf{k}) = \int_0^Z \frac{dk}{k} \frac{\mathbf{W}(\mathbf{k} D)^2}{k} \mathbf{J}_2(t \mathbf{k} D); \quad (59)$$

For the angular top-hat filter, given by eq.(15) in Fourier space, we can perform the integration over \mathbf{k}_1 in eq.(58), using the standard properties of Bessel functions, and we obtain:

$$h_{1s}^p i_c = S_p \int_0^Z \int_1^Z \frac{dt}{t} \frac{d}{2} (\hat{w} \cos 2 \int \mathbf{k}_1)^p I_1^{p-1}; \quad (60)$$

Here we have dropped the minus sign in front of the factor $\cos 2 \int \mathbf{k}_1$ because all odd moments vanish, as seen by integration over t . Thus, we recover the fact that the PDF, $P(1)$, is even, which was obvious from the definition of the shear since there is no preferred direction in the system.

Finally, the expression (60) allows us to obtain the generating function $\hat{h}_{1s}^p(y)$ of the shear component h_{1s}^p , defined as in eq.(23), using the resummation (28) (where we replace S_p by S_p ; see eq.(49)):

$$\hat{h}_{1s}^p(y) = \int_0^Z \int_1^Z \frac{dt}{t} \frac{d}{2} \frac{\hat{h}_{1s}^p}{I_1} \frac{y \cos 2 \int \mathbf{k}_1}{\hat{h}_{1s}^p} \hat{w}; \quad (61)$$

Here we have introduced the variance $\hat{h}_{1s}^2 = h_{1s}^2 i$. From eq.(60) it is given by:

$$\hat{h}_{1s}^2 = \int_0^Z \int_1^Z \frac{dt}{t} \frac{d}{2} (\hat{w} \cos 2 \int \mathbf{k}_1)^2 I_1 = \frac{1}{2} \int_0^Z \int_0^Z \frac{dk}{k} \frac{\mathbf{W}(\mathbf{k} D)^2}{k} \mathbf{J}_2(t \mathbf{k} D); \quad (62)$$

Here we have used $S_2 = 1$; see eq.(41), which is still verified by our parameterization (42). Of course, eq.(62) is exact, within the small-angle approximation, and the last equality in eq.(62) shows that we recover the property $\hat{h}_{1s}^2 i = h_{1s}^2 i = 2$. For the shear component h_{2s}^p , we obtain the same equations with $\cos 2 \int \mathbf{k}_1$ replaced by $\sin 2 \int \mathbf{k}_1$. This leaves the cumulants $h_{2s}^p i_c = h_{1s}^p i_c$ unchanged and we get the same generating function. Therefore, we recover $P(1) = P(2)$. Finally, the PDF is given by the inverse Laplace transform (24):

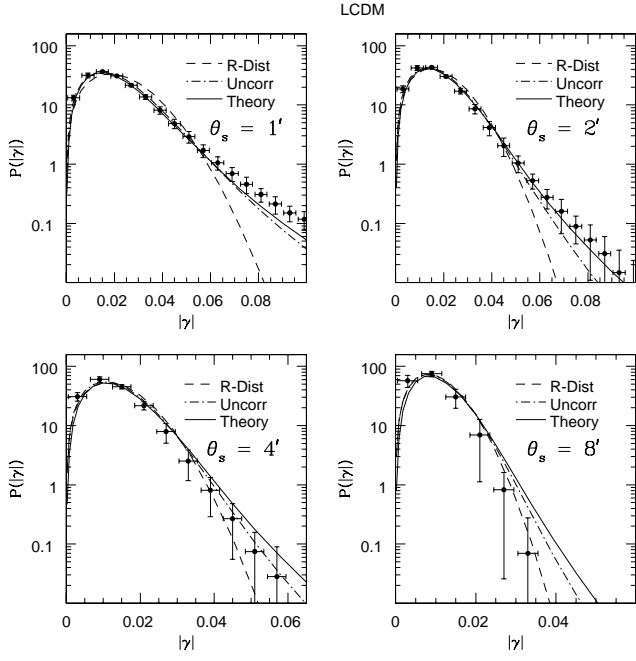


Figure 4. Probability distribution function, $P(j)$, for the LCDM cosmology, plotted as a function of j . The smoothening angle, θ_s , varies from 1° (upper left panel) to 8° (lower right panel). The data-points are the results from the numerical simulations and the solid lines correspond to the analytical predictions (67), (73) and (74) based on our stellar model. The dashed lines are the predictions obtained by assuming that both the shear components, γ_1 and γ_2 , are uncorrelated Gaussian variables, with the correct variance (this yields a Rayleigh distribution for j). The dotted-dashed curve also assumes that the two shear components are uncorrelated but their PDF is given by our non-linear prediction; this corresponds to eqs.(75) and (76). The source redshift is fixed at unity in each case.

$$P(\hat{\gamma}_{1s}) = \frac{1}{2} \int_{-\infty}^{\infty} \frac{dy}{i \hat{\gamma}_{1s}} e^{[\hat{\gamma}_{1s} y - \hat{\gamma}_{1s}^2(y)]} = \hat{\gamma}_{1s} : \quad (63)$$

The generating function $\hat{\gamma}_{1s}(y)$ obtained in Section 3.4 shows a branch cut along the negative real axis for $y < y_s$; see eq.(50). Then, we see from eq.(61) that the generating function $\hat{\gamma}_{1s}(y)$ for the shear component γ_1 shows two symmetric branch cuts along the real axis, for $y < -y_s \hat{\gamma}_{1s}$ and $y > y_s \hat{\gamma}_{1s}$, with:

$$y_s \hat{\gamma}_{1s} = \frac{\hat{\gamma}_{1s} j}{\max_{\hat{w}} \frac{I_1}{\hat{w}} \hat{\gamma}_{1s}} : \quad (64)$$

This implies an exponential tail for $P(\hat{\gamma}_{1s})$ at large $\hat{\gamma}_{1s} j$:

$$\hat{\gamma}_{1s} j \gg 1 : P(\hat{\gamma}_{1s}) \propto e^{y_s \hat{\gamma}_{1s} \hat{\gamma}_{1s} j} \propto e^{-\hat{\gamma}_{1s} j} ; \quad (65)$$

which translates into similar exponential tails for the shear $\gamma_1 = j \hat{\gamma}_{1s}$ in $\hat{\gamma}_{1s}$. Finally, the typical wavenumber k and redshift z used in eq.(46) are defined as the point (k, z) , which maximizes the contribution to $\hat{w} I_1 = \hat{\gamma}_{1s}$ (see eq.(64)) that is the location of the maximum over k, z and t of $\hat{w}(z)W(kD)J_2(tkD)^2(k, z) = k$ (see eq.(59)).

4.2 PDF of the shear modulus, $j j$

From the smoothed shear components, $\hat{\gamma}_{1s}$ and $\hat{\gamma}_{2s}$, we may define the smoothed modulus, $\hat{j}_{s,j}$ as:

$$\hat{j}_{s,j} = \hat{j}_{1s} + i \hat{\gamma}_{2s} j = \frac{P}{\hat{\gamma}_{1s}^2 + \hat{\gamma}_{2s}^2} : \quad (66)$$

Note that eq.(66) means that we take the modulus of the shear after smoothing of the two components, γ_1 and γ_2 . Since smoothing and taking the modulus do not commute, the quantity $\hat{j}_{s,j}$ defined in eq.(66) is not the smoothed shear obtained by first taking the modulus $j = j_1 + i j_2$ at each point on the sky and second applying a top-hat smoothing to this map. In this paper we shall only consider the smoothed modulus $\hat{j}_{s,j}$ as defined in eq.(66). Indeed, since taking the modulus is a non-linear process one cannot directly apply the method used in this paper to derive the PDF of the modulus defined by first taking the modulus of the shear. By contrast, we can easily study the smoothed modulus $\hat{j}_{s,j}$ defined in eq.(66) because it can be directly obtained from the properties of the smoothed shear components, $\hat{\gamma}_{1s}$ and $\hat{\gamma}_{2s}$. Indeed, from eq.(66) we obtain the relation:

$$Z_2 P(\hat{j}_{s,j}) = \hat{j}_{s,j} d P(\hat{j}_{s,j} \cos \theta_s; \hat{j}_{s,j} \sin \theta_s) ; \quad (67)$$

where we have introduced the joint PDF, $P(\hat{\gamma}_{1s}; \hat{\gamma}_{2s})$, of the two shear components, $\hat{\gamma}_{1s}$ and $\hat{\gamma}_{2s}$. Of course, following the method used in Section 4.1 for the shear components we can obtain the joint PDF, $P(\hat{\gamma}_{1s}; \hat{\gamma}_{2s})$, from the cumulants, $h_{1s}^{p_1} h_{2s}^{p_2} i_c$. Thus, proceeding along the lines of Section 4.1 the analog of eq.(60) now reads:

$$h_{1s}^{p_1} h_{2s}^{p_2} i_c = S_{p_1 + p_2} \int_0^{\infty} \int_1^{\infty} \frac{dt}{t} \frac{d}{t} \left(\cos^2 \theta_s (\sin 2 \theta_s I_1^{p_1 + p_2})^1 \right) : \quad (68)$$

Then, the generating function, $\hat{\gamma}_{1s}; \hat{\gamma}_{2s}(y_1; y_2)$, defined as in eq.(22) by:

$$\hat{\gamma}_{1s}; \hat{\gamma}_{2s}(y_1; y_2) = \frac{\int_0^{\infty} \int_1^{\infty} \frac{dt}{t} \frac{d}{t} y_1^{p_1} y_2^{p_2}}{p_1! p_2!} h_{1s}^{p_1} h_{2s}^{p_2} i_c y_1^{p_1} y_2^{p_2} \quad (69)$$

can be written from eq.(68) as:

$$\hat{\gamma}_{1s}; \hat{\gamma}_{2s}(y_1; y_2) = \int_0^{\infty} \int_1^{\infty} \frac{dt}{t} \frac{d}{t} \frac{1}{I_1} \frac{1}{p_1! p_2!} S_p (I_1 \hat{w})^p (y_1 \cos 2 \theta_s + y_2 \sin 2 \theta_s)^p : \quad (70)$$

Using the resummation (28) we get:

$$\hat{\gamma}_{1s}; \hat{\gamma}_{2s}(y_1; y_2) = \int_0^{\infty} \int_1^{\infty} \frac{dt}{t} \frac{d}{t} \frac{1}{I_1} \frac{1}{p_1! p_2!} (y_1 \cos 2 \theta_s + y_2 \sin 2 \theta_s) I_1 \hat{w} : \quad (71)$$

Next, from the cumulant generating function, $\hat{\gamma}_{1s}; \hat{\gamma}_{2s}$, we define the normalized generating function, $\hat{\gamma}_{1s}; \hat{\gamma}_{2s}$, by:

$$\hat{\gamma}_{1s}; \hat{\gamma}_{2s}(y_1; y_2) = \hat{\gamma}_{1s} \hat{\gamma}_{1s}; \hat{\gamma}_{2s} \frac{y_1}{\hat{\gamma}_{1s}}; \frac{y_2}{\hat{\gamma}_{1s}} \quad (72)$$

and eq.(71) yields:

$$\hat{\gamma}_{1s}; \hat{\gamma}_{2s}(y_1; y_2) = \int_0^{\infty} \int_1^{\infty} \frac{dt}{t} \frac{d}{t} \frac{1}{I_1} \frac{\hat{\gamma}_{1s}}{I_1} : \quad (73)$$

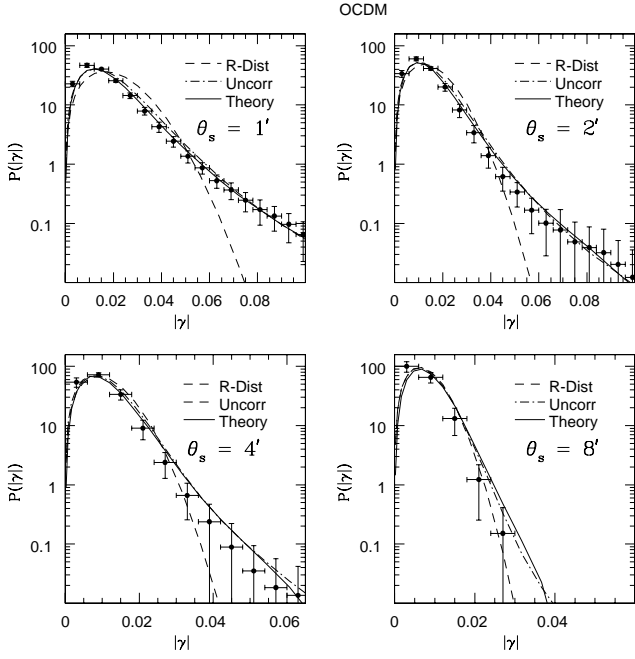


Figure 5. As for the previous Figure, but for the OCDM cosmology.

$$' (y_1 \cos 2 + y_2 \sin 2) \frac{I_1}{\hat{\gamma}_{1s}} \hat{w} : \quad (73)$$

Then, the joint PDF, $P(\hat{\gamma}_{1s}; \hat{\gamma}_{2s})$, is given by:

$$P(\hat{\gamma}_{1s}; \hat{\gamma}_{2s}) = \frac{Z_{+ii}}{i!} \frac{dy_1 dy_2}{(2 \hat{\gamma}_{1s})^2} e^{[\hat{\gamma}_{1s} y_1 + \hat{\gamma}_{2s} y_2 - \hat{\gamma}_{1s} \hat{\gamma}_{2s} (y_1 y_2)]} = \hat{\gamma}_{1s} : \quad (74)$$

It is interesting to compare our results (73) and (74) with the prediction we would obtain if we had assumed that $\hat{\gamma}_{1s}$ and $\hat{\gamma}_{2s}$ were uncorrelated, but still described by the PDF derived in Section 4.1. Then, the normalized generating function, $' \hat{\gamma}_{1s} \hat{\gamma}_{2s} (y_1; y_2)$ would simply be given by:

$$' \hat{\gamma}_{1s} \hat{\gamma}_{2s} (y_1; y_2) = ' \hat{\gamma}_{1s} (y_1) + ' \hat{\gamma}_{2s} (y_2) : \quad (75)$$

Substituting this into eq.(74), we obviously recover the property:

$$P^{\text{uncorr}}(\hat{\gamma}_{1s}; \hat{\gamma}_{2s}) = P(\hat{\gamma}_{1s})P(\hat{\gamma}_{2s}) : \quad (76)$$

Therefore, the fact that $' \hat{\gamma}_{1s} \hat{\gamma}_{2s}$ obtained in eq.(73) cannot be written as the sum (75) shows that within our stellar model of Section 3.3.2 for the density field, both shear components, $\hat{\gamma}_{1s}$ and $\hat{\gamma}_{2s}$, are correlated, which is actually quite natural. Moreover, the comparison of (74) with (76) will allow us to study numerically the influence of these correlations onto the PDF of the smoothed modulus $\hat{\gamma}_s$.

5 LEN SING STATISTICS FROM NUMERICAL SIMULATIONS

We compare in the following Section our analytical results for the shear with weak lensing statistics obtained in cosmological N-body simulations. Couchman, Barber & Thomas

Table 1. Cosmological and simulation parameters characterizing the different models

	m	8	res	survey
LCDM	0.25	0.3	0.7	1.22
OCDM	0.25	0.3	0.0	1.06

(1999) developed an algorithm for computing the shear in three dimensions at locations within the simulation volumes and we have applied this algorithm to the simulations of the Hydra Consortium² produced using the Hydra N-body hydrodynamics code (Couchman, Thomas & Pearce, 1995).

We used two simulations, a flat cosmology with a cosmological constant and an open cosmology with zero cosmological constant. These will be referred to as the LCDM and OCDM cosmologies, respectively. Both contained dark matter particles only of mass $1.29 \times 10^{11} h^{-1}$ solar masses, where h expresses the value of the Hubble parameter in units of $100 \text{ km s}^{-1} \text{ Mpc}^{-1}$. The number of particles in each cosmology was 86^3 . We used a variable particle softening in the code with a minimum value in box units of $0.007(1+z)$, where z is the redshift of the simulation volume. The simulation volumes had comoving side-dimensions of $100 h^{-1} \text{ Mpc}$. To avoid obvious structure correlations between adjacent boxes, each was arbitrarily translated, rotated (by multiples of 90°) and reflected about each coordinate axis, and in addition, each complete run was performed 10 times in each cosmology. The cosmological and simulation parameters of both the LCDM and OCDM simulations are given in Table 1.

The general procedure for specifying the coordinates for the lines-of-sight and the locations within the simulations for the computations of the 3-d shear is as described by Barber (2002). In the present work, a total of 455 lines of sight were used which completely filled the simulation box immediately preceding the one at redshift 1 and allowed regular sampling of the field of view. In addition, 300 regularly-spaced evaluation locations for the shear along each line of sight were specified in each simulation volume to adequately sample the varying gravitational potential. In the LCDM cosmology, the full field of view was 2.6×2.6 and in the OCDM cosmology, 2.8×2.8 . The angular resolution in the LCDM cosmology was 0.34° , which equates to the minimum value of the particle softening at the optimum redshift, $z = 0.36$, for lensing of sources at a redshift of 1. In the case of the OCDM cosmology, the angular resolution was 0.37° . In both cosmologies, to allow for the larger angular size of the minimum softening at low redshifts and also for the range of particle softening scales above the minimum value, we have not declared our results below angular scales of 1 arcminute.

To obtain the lensing statistics for sources at redshift $z_s = 1$, we computed the required values assuming the sources were located at the front face of the simulation volume whose redshift was closest to 1. Therefore in the LCDM cosmology, the sources were at $z_s = 0.99$ and in the OCDM cosmology they were at $z_s = 1.03$.

² (<http://hydra.mcmaster.ca/hydra/index.htm>)

Once the 3-d shear had been computed at each location, the multiple lens-plane theory, described clearly in Schneider, Ehlers & Falco (1992), was applied along the lines of sight. The procedure involved combining the intermediate Jacobian matrices computed using the appropriate values of the angular diameter distances in the relevant cosmology. Finally, the Jacobian matrices appropriate at $z = 0$ for sources at $z_s = 1$ for every line of sight were obtained.

From the Jacobian matrices in each of the 10 simulation runs for each cosmology, we computed the shear components, γ_1 and γ_2 , and the full shear, γ . The values for the smoothed components were computed on angular scales of $1^0.0, 2^0.0, 4^0.0$ and $8^0.0$, using a top-hat filter.

The computed values for the probability distributions from each of the $N = 10$ runs in each cosmology were averaged, and the errors on the means of $1 = N$ determined.

6 COMPARISON OF ANALYTICAL PREDICTIONS WITH RESULTS FROM NUMERICAL SIMULATIONS

We compare here our analytical predictions for the smoothed shear components and for the shear modulus with the results of the numerical simulations. The quantities plotted are for various smoothing angles from 1^0 to 8^0 in the two different cosmologies, LCDM and OCDM, and in each case the source redshift is fixed at unity.

Firstly we compare the results for the shear components, plotted in Figure 2, for the LCDM cosmology, and Figure 3, for the OCDM cosmology. Since the PDFs for the components are even functions we only plot the PDF, $P(\gamma_1)$, over $\gamma_1 \geq 0$. The solid lines correspond to our analytical predictions, (61) and (63), based on the stellar model. For comparison, we also plot the Gaussian distribution which has the same variance (the dashed curves), so as to clearly show the deviations from Gaussianity. We find that at small angular scales, $\theta_s \leq 4^0$, the results from the numerical simulations are very accurately described by our non-linear predictions where there are clear signs of departure from Gaussianity, especially in the tails of the PDF. Of course, this merely reflects the non-linearity of the underlying mass distribution probed by these small angular windows. At larger smoothing angles, $\theta_s > 4^0$, the stellar Ansatz seems to over-predict the non-linearity induced by gravitational clustering and the results lie between the fully non-linear predictions and the Gaussian approximations. This behaviour can be due to the fact that such large angular windows probe the transition between the linear and highly non-linear regimes for the underlying density field. This intermediate case is more difficult to handle because the parameters S_p (e.g., the skewness) exhibit a strong variation with redshift and scale during this phase (while they remain almost constant within the linear and highly non-linear regimes). Therefore, a simple mean as in eq.(46) may be insufficient to provide very accurate results. We did not try in this work to improve over the simple interpolation of eq.(46) because we expect the stellar model to be less accurate in the quasi-linear regime. Indeed, in the quasi-linear regime the angular dependence of the many-body correlations can be derived from perturbation theory and one can see that for the three-point function it already violates eqs.(38)–(41). On the other hand, in

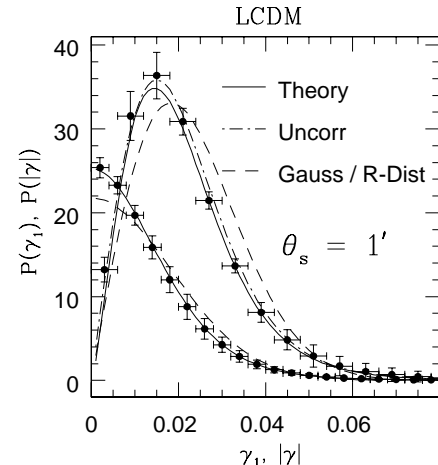


Figure 6. The PDFs, $P(\gamma_1)$ and $P(\gamma_2)$, on a linear scale for the LCDM cosmology and smoothing angle $\theta_s = 1^0$. The source redshift is again fixed at unity. The curves and the data-points are the same as in the upper left panels of Figures 2 and 4.

the highly non-linear regime, the angular dependence of the many-body correlations gets shallower and eqs.(38)–(41) actually agree with numerical simulations for the three-point function (Scoccimarro & Frieman 1999).

The PDFs for the shear modulus are presented in Figure 4, for the LCDM cosmology, and Figure 5, for the OCDM cosmology. The solid lines show our analytical predictions (67)–(73)–(74) from the stellar model. For comparison, we also plot (dotted-dashed curves) the results obtained by assuming that the two shear components are uncorrelated but their own PDFs are still given by our non-linear prediction; this corresponds to eqs.(75)–(76). Therefore, we see from Figures 4 and 5 that the correlation between both components, γ_1 and γ_2 , only has a rather small influence on the PDF of the modulus, $P(\gamma)$. For reference we have also shown the results for the uncorrelated Gaussian case (dashed curves), where the PDF for γ is given by a Rayleigh distribution with a variance equal to that of the shear components (dashed curves). Comparison of our predictions with the results of the numerical simulations shows that there is a remarkable agreement in both cosmologies (as found for the shear components), especially at the smaller smoothing scales. At the larger scales, the agreement is less good for the same reasons as described above. The sample variance arising from the various realisations also makes the comparison more difficult; as the size of the smoothing radius is increased, the number of patches with completely independent information decreases, thereby increasing the sample variance. In addition, although we made use of 10 different simulation runs (as described in Section 5), they were all based upon the same N -body realisation in each cosmology, so the separate runs may not contain completely independent information. Much larger simulations would be required to quantify any departure from the analytical predictions.

Finally, we display in Figure 6 our results over a linear scale for P rather than the logarithmic scale of the previous Figures, for the LCDM cosmology and the smoothing angle $\theta_s = 1^0$. While the previous Figures emphasized the tails of the PDFs we can clearly see in Figure 6 the shapes of the

PDFs near their maximum. In agreement with the discussion above, we can check that our predictions match the deviations from Gaussianity observed in the numerical simulations. Thus, the PDF, $P(1)$, of the shear component, γ_1 , is more sharply peaked around $\gamma_1 = 0$ than a Gaussian. Moreover, the location of the maximum of the PDF, $P(j)$, of the shear modulus is accurately reproduced by our analytical model. These features might be useful, in addition to the extended tails seen in the previous Figures, to measure in weak lensing surveys the departures from Gaussianity brought by the non-linear gravitational dynamics. This may also help to break the degeneracies in the measurement of the cosmological parameters.

7 DISCUSSION

Extending earlier studies we have developed analytical techniques based on a simple hierarchical Ansatz, which we called the stellar model, to compute various statistical quantities associated with cosmic shear. Thus, we have computed the full probability distribution functions associated with the smoothed shear components, $P(\gamma_1(s))$, and the modulus of cosmic shear, $P(j(s))$. Here $j(s)$ is defined by first smoothing both shear components and second taking their modulus. We have also derived the joint-PDF, $P(\gamma_1(s); \gamma_2(s))$. These results extend similar studies applied to the convergence field. However, being a spin-2 field, statistics from the shear are much richer than those from the convergence field and, more importantly, can be directly used for observational purposes where the non-trivial survey geometry can pose a considerable problem for reconstructing convergence (γ) maps.

The comparison of our analytical calculations with the results of the numerical simulations shows that our simple method yields accurate predictions at small angular scales, $s \gtrsim 4'$ (for a source redshift $z_s = 1$) which probe the non-linear regime for the underlying density field. Therefore, we can use with confidence the simple stellar model we introduced in this paper to study the shear statistics and extract useful information from future surveys. In particular, our analysis shows how the deviations from Gaussianity in the density field built by the non-linear gravitational dynamics translate into the PDF of the shear. This can also be seen in the Figures where we drew Gaussian PDFs for comparison. Hence we may hope to derive from shear maps some key properties of the structure of the density field (e.g., the amplitude of the many-body correlations and the shape of the PDF of the smoothed density contrast) which could shed some light onto the non-linear regime of gravitational clustering. In this respect, note that the separation of the shear, γ , into the factor γ_{lin} and the "normalized shear," γ^* , also provides a good separation between the dependence on the cosmological parameters and the projection effects (e.g., $\gamma_{\text{lin}}; \gamma^*$ and z_s) versus the non-Gaussianities of the density field which characterize the collisionless gravitational dynamics itself. This is obvious for the convergence, γ_0 , as recalled at the end of Section 3.2, but this feature also holds for the shear, γ .

However, in the near future, where the observational noise may still be important, one may first focus on the estimation of the cosmological parameters. To this order, our

study is complementary to present analysis of the first few higher-order correlation functions of the shear field (Zaldarriaga & Scoccimarro, 2003, Schneider & Lombardi, 2003, Bernardeau, Van Waerbeke & Mellier, 2002, and Masahiro & Jain 2003) based on results derived for cosmological spin-2 fields such as CMB polarization, where shape dependence and scale dependence of the shear is used to study non-Gaussianity induced by the underlying mass distribution. In any case, a few measures of non-Gaussianity (e.g., the skewness of the convergence, γ_0) are useful to remove degeneracies between the various cosmological parameters (e.g., γ_0 vs γ_1) since a Gaussian is defined by only one quantity (its variance), while we would like to measure several quantities. Therefore, one may use our prediction for the PDF, $P(\gamma)$, to build some useful new observables.

Before we can use our method to extract some information from weak gravitational lensing surveys, there are some points which need to be addressed. In particular, we should take into account the effects of a finite width for the distribution of sources over redshift, as in actual surveys. It would also be desirable to include realistic noise, such as that arising from the intrinsic ellipticity distribution of galaxies, and Poisson sampling due to the discreteness of the source distribution. The finite size of the catalogue is also worthy of consideration. These effects are beyond the scope of this paper, where we have mainly investigated the accuracy of our approach to describe the physics of weak gravitational lensing by large-scale structures. Having shown here that our simple stellar model provides a useful basis, we plan to investigate these points in detail in future work.

On the other hand, the present study already gives some information about delicate points which are of theoretical and practical interest. In particular, the underlying approximation in most analytical calculations (including ours) is the Born approximation. It neglects higher order correction terms in the photon propagation equation. The error introduced by such an approximation in the quasi-linear regime has been studied by several authors (e.g. Schneider et al. 1998). Although perturbative calculations tend to show that this error is negligible for lower order cumulants, clearly such an analysis is not possible in the highly non-linear regime. However, previous studies of convergence statistics and our present results regarding the shear PDF, which exhibit a good match between theoretical predictions and the simulation results, indicate that such corrections are negligible even in the highly non-linear regime.

With regard to numerical simulations, previous work for the predicted convergence statistics were made in comparison with ray-tracing experiments. In the present case, our analytical results for the shear, which are complementary to the convergence results, are compared successfully with the numerical computations based on computing the full 3-d shear along every line of sight. The detailed match of our various predictions not only verifies our analytical calculations but also increases our confidence in the two different numerical methods.

8 ACKNOWLEDGEMENTS

This work has been supported by PPARC and the numerical work carried out with facilities provided by the University

of Sussex. A JB was supported in part by the Leverhulme Trust. The original code for the 3-d shear computations was written by Hugh Couchman of M cMaster University. There were many useful discussions with Antonio da Silva. DM acknowledges the support from PPARC of grant RG 28936. DM also acknowledges support from the University of Sussex during a visit where part of the work was completed. It is a pleasure for DM to acknowledge many fruitful discussions with members of Cambridge Leverhulme Quantitative Cosmology Group, including Jerry Ostriker and Alexandre Refregier.

REFE RENCES

Babul A., Lee M. H., 1991, MNRAS, 250, 407
 Barber A. J., Taylor A. N., 2002, submitted to MNRAS, (astro-ph/0212378)
 Barber A. J., MNRAS, 2002, 335, 909
 Bacon D. J., Refregier A., Ellis R. S., 2000, MNRAS, 318, 625
 Balian, R., Schaefer, R., 1989, A&A, 220, 1
 Bartelmann M., Huh H., Colberg J. M., Jenkins A.
 Bartelmann, M., Schneider, P., 2001, Physics Reports, 340, 291B
 Bernardeau, F., 1994, A&A, 291, 697
 Bernardeau, F., Schaefer, R., 1992, A&A, 255, 1
 Bernardeau, F., Valageas, P., 2000, A&A, 364, 1
 Bernardeau, F., Van Waerbeke, L., Mellié, Y., 1997, A&A, 322, 1
 Bernardeau, F., Van Waerbeke, L., Mellié, Y., 2002, 389, L28-L32
 Blandford R. D., Saust A. B., Brainerd T. G., Villumsen J. V., 1991, MNRAS, 251, 600
 Boschan P., Szapudi I., Szalay A. S., 1994, ApJS, 93, 65
 Colombi, S., Bouchet, F. R., Schaefer, R., 1995, ApJS, 96, 401
 Colombi S., Bouchet, F. R., Hernquist, L., 1996, ApJ, 465, 14
 Couchman, H. M. P., Barber, A. J., Thomas, P. A., 1999, MNRAS, 308, 180
 Couchman, H. M. P., Thomas, P. A., Pearce, F. R., 1995, ApJ., 452, 797
 Davis M., Peebles P. J. E., 1977, ApJS, 34, 425
 Fry, J. N., 1984, ApJ, 279, 499
 Fry, J. N., Peebles, P. J. E., 1978, ApJ, 221, 19
 Grotth, E., Peebles, P. J. E., 1977, ApJ, 217, 385
 Gunn, J. E., 1967, ApJ, 147, 61
 Hamilton A. J. S., Kumar, P., Lu, E., Matthews, A., 1991, ApJ, 374, L1
 Hoekstra H., Yee H. K. C., Gladders, M. D., 2002, ApJ, 577, 595
 Hui L., 1999, ApJ, 519, 622
 Jain B., Mo H. J., White S. D. M., 1995, MNRAS, 276, L25
 Jain, B., Seljak, U., 1997, ApJ, 484, 560
 Takada M., Jain B., 2002, MNRAS, 337, 875
 Jain B., Van Waerbeke L., 1999, astro-ph/9910459
 Jain B., Seljak U., White S. D. M., 2000, ApJ, 530, 547
 Jannink, G., Des Cloiseaux, J., 1987, Les polymères en solution, Les éditions de physique, Les Ulis, France
 Jaroszyn'ski M., Park C., Paczynski B., Gott J. R., 1990, ApJ, 365, 22
 Jaroszyn'ski M., 1991, MNRAS, 249, 430
 Kaiser N., 1992, ApJ, 388, 272
 Kaiser N., 1998, ApJ, 498, 26
 Linber D. N., 1954, ApJ, 119, 665
 Lee M. H., Paczyn'ski B., 1990, ApJ, 357, 32
 Masahiro T., Jain B., 2003, ApJ, 583, L49
 Miralda-Escude J., 1991, ApJ, 380, 1
 Munshi D., Bernardeau F., Mellié A. L., Schaefer R., 1999, MNRAS, 303, 433
 Munshi D., Coles P., Mellié A. L., 1999a, MNRAS, 307, 387
 Munshi D., Coles P., Mellié A. L., 1999b, MNRAS, 310, 892
 Munshi D., Mellié A. L., Coles P., 1999, MNRAS, 311, 149
 Munshi D., Coles P., 2000, MNRAS, 313, 148
 Munshi D., Coles P., 2002, MNRAS, 329, 797
 Munshi D., Coles P., 2003, MNRAS, 338, 846
 Munshi D., Jain B., 2000, MNRAS, 318, 109
 Munshi D., Jain B., 2001, MNRAS, 322, 107
 Munshi D., 2000, MNRAS, 318, 145
 Wang Y., Holz D. E., Munshi D., 2002, ApJ, 572L, 15
 Peebles, P. J. E., 1980, The large scale structure of the universe, Princeton University Press
 Peacock J. A., Dodds S. J., 1994, Peacock J. A., Dodds S. J., 1996, MNRAS, 280, L19
 Remaldi M., Martel H., Matzner R., 1998, ApJ, 493, 10
 Schaefer, R., 1984, A&A, 134, L15
 Schneider, P., Ehlers, J., Falco, E. E., 1992, Gravitational Lenses, Springer-Verlag, ISBN 0-387-97070-3
 Schneider P., Weiss A., 1988, ApJ, 330, 1
 Schneider P., Lombardi M., 2003, A&A, 397, 809
 Schneider P., Van Waerbeke L., Jain B., Knezevic, 1998, MNRAS, 296, 873, 873
 Scoccimarro R., Colombi S., Fry J. N., Frieman J. A., Hivon E., Mellié A. L., 1998, ApJ, 496, 586
 Scoccimarro R., Frieman J. A., 1999, ApJ, 520, 35
 Scoccimarro R., Zaldarriaga M., 2003, ApJ, 584, 559
 Stebbins A., 1996, astro-ph/9609149
 Szapudi I., Szalay A. S., 1993, ApJ, 408, 43
 Szapudi I., Szalay A. S., 1997, ApJ, 481, L1
 Valageas P., Schaefer, R., 1997, A&A, 328, 435
 Valageas P., 2000a, A&A, 354, 767
 Valageas P., 2000b, A&A, 356, 771
 Valageas P., 2002a, A&A, 382, 412
 Valageas P., 2002b, A&A, 382, 477
 Van Waerbeke L., Bernardeau F., Mellié Y., 1999, A&A, 342, 15
 Van Waerbeke L., Mellié Y., Pello, R., Pen U. L., Mccracken H. J., Jain B., 2002, A&A, 393, 369
 Van Waerbeke, L., et al., 2000, A&A, 358, 30
 Villumsen J. V., 1996, MNRAS, 281, 369
 Whitegang J., Cen R., Ostriker J. P., 1998, ApJ, 494, 298
 Whitegang J., Cen R., Xu G., Ostriker J. P., 1997, ApJ, 494, 29
 Whitegang J., Cen R., Ostriker J. P., Turner E. L., 1995, Science, 268, 274
 Wang Y., Holz D. E., Munshi D., 2002, ApJ, 572L, 15
 White M., Hu W., 2000, ApJ, 537, 1
 Zaldarriaga M., Scoccimarro R., 2003 ApJ, 584, 559